Fast Dynamics of Ionization in Ultraviolet Matrix-Assisted Laser Desorption Ionization of Biomolecules

Eugene Moskovets and Akos Vertes*

Department of Chemistry, The George Washington University, Washington, D.C. 20052

Received: August 7, 2001; In Final Form: December 27, 2001

The kinetics of guest ion formation in matrix-assisted laser desorption ionization was studied for substance P and insulin from 2,5-dihydroxybenzoic acid (DHB), α-cyano-4-hydroxycinnamic acid (CHCA), 9-anthracenecarboxylic acid (9-ACA), and sinapinic acid (SA) matrixes. The results show two very different responses. Although guest ion yields from DHB and SA follow a simple fast exponential decay (with decay times of 4.3 ± 0.7 ns and 4.6 ± 0.8 ns, respectively), the ions from the other two matrixes show extended maxima (at 6.1 ns for CHCA and 3.2 ns for 9-ACA) with only a moderate decline in their yield. Possible explanations for the fast exponential decay include the relaxation of electronically and/or vibrationally excited matrix precursors for DHB and SA. The explanation of extended maxima in the case of 9-ACA and especially CHCA can be based on competition for the protons between matrix and guest species. CHCA has significantly lower proton affinity than SA, thus, resulting in lower deprotonation rates for guest ions. There is, however, an alternative explanation. As long as the matrix surface temperature exceeds the sublimation temperature, there is sufficient vaporization to sustain a dense MALDI plume and facilitate guest ionization.

Introduction

In recent years, matrix-assisted desorption ionization (MALDI) has rapidly evolved from a novel and obscure technique to a common application that is considered routine by researchers in various fields. Due to sustained efforts of multiple research groups, it continues to provide unique analytical data for diverse classes of bio- and synthetic polymers. The origin of ions produced by MALDI, however, continues to be the subject of scientific debate.[1] The complexity of MALDI stems from the fact that it is the result of several simultaneous and consecutive processes occurring during a vigorous phase transition initiated by the laser pulse. Although the focus of mechanistic studies into MALDI has been to provide an explanation for guest ion formation, it is equally important to understand the production of other species, e.g., matrix ions. In most of the proposed models, these two processes are intimately coupled.

Typical polar organic molecules used as MALDI matrixes have ionization potentials (IP) in the 8−9 eV range.[2] Because the total energy in two 337 nm quanta (2 × 3.68 eV = 7.36 eV) is below the IP of the matrix molecules in the gas phase, the energy deficit for matrix photoionization has to be accounted for. One set of potential explanations is based on IP-lowering effects. According to an early model, photoionization can take place only in the solid phase where the IP is lowered by 1 to 1.5 eV due to polarization forces. The same forces are invoked to explain the red shift in the absorption band of matrix molecules in crystalline films.[3] In the polar fluid model, the production of protonated guest molecules is explained by the solvating effect of the overheated fluid matrix, present before substantial plume expansion takes place.[4] The guest molecules are immersed into this environment and guest ions are produced by proton-transfer reactions facilitated by solvent polarization. In this mechanism, polarization forces lead to a reduction in the activation barrier of the proton-transfer reaction.

To account for commonly observed protonated guest molecules several potential reactions have been proposed: the excited-state proton transfer (ESPT) between the excited matrix molecule and neutral guest molecule,[5−7] ion−molecule reactions between matrix radical cations and the guest,[8] matrix cation to guest proton transfer,[9] protonated matrix to guest proton transfer[10,11] and intracluster proton transfer.[12,13]

In another set of models, the energy deficit is made up by thermal or cooperative effects. In the photothermal model, the thermal activation of the matrix is a prerequisite to obtain a photoionized molecule. This may be a relatively efficient process since in the expanding plume matrix molecules acquire a mean translational energy close to half of an eV[2]. Due to the generation of highly mobile excited states in the matrix, the solid-state pooling of excitons is possible and can supply the energy necessary for ionization.[14]

By following the kinetics of ion production for the various species, it is possible to reduce the number of potential explanations. Both matrix and guest ionization, as well as plume expansion occur on the ps to ns time scale. Most of these events are over in less than 50 ns. Thus, it is desirable to monitor the kinetics of ion formation within the same time frame. Pump−probe experiments are widely used to study fast reactions and relaxation processes with up to ∼10 fs time resolution. In an earlier study, we used two laser pulses from nitrogen lasers to study *guest ion formation* kinetics on the ns time scale.[15] Although it was clear that in most cases the guest ion yield did not follow a simple exponential decay, due to significant jitter between the pump and probe pulses it was difficult to discern the functional form of the time dependence of the ion yield. In a similar study, we utilized a mode-locked Nd:YAG laser and an optical delay line to explore *matrix ion yields* with ∼30 ps time resolution.[16] Although various trends in the ion yield as a

* To whom correspondence should be addressed. Phone: (202) 994−2717. Fax: (202) 994−5873. E-mail: vertes@gwu.edu.

10.1021/jp013027t CCC: $22.00
Published on Web 03/05/2002

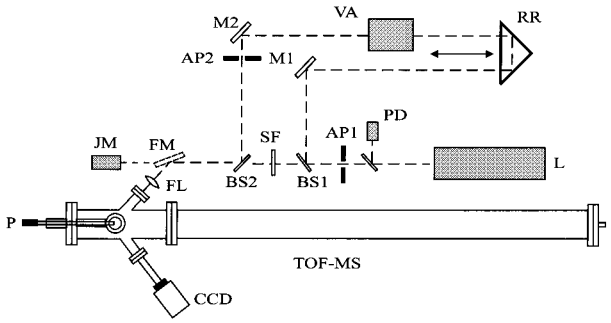

Figure 1. Schematic layout of the MALDI pump−probe experiments. The system components included: beam splitters (BS1 and BS2), mirrors (M1 and M2), iris apertures (AP1 and AP2), retroreflector (RR), variable attenuator (VA), step filter (SF), flip mirror (FM), joulemeter (JM), photodiode (PD), focusing lens (FL), laser (L), time-of-flight mass spectrometer (TOF-MS), solid insertion probe (P) and aligning camera (CCD). The delay time between the direct and delayed pulses was changed by translating the retroreflector along the beam axis.

function of delay time were obvious, the substantial scatter in the data did not permit us to establish a functional relationship.

Hydrodynamic calculations describe the MALDI plume as an expanding system with two distinct regimes.[17] In the first regime the surface temperature, T_{surf}, of the sample is lower than the phase transition (in most cases sublimation) temperature, T_{subl}. During this regime, there is negligible material transport across the interface and only a hot spot is created on the sample surface. In the second regime ($T_{surf} > T_{subl}$), a significant stream of material enters the plume. These two regimes are present during the laser-heating phase and in reverse order they are also active after the end of the laser pulse. In other words, the material balance of the plume changes dramatically following the laser pulse as the temperature of the cooling surface drops below T_{subl}. This transition marks the beginning of plume detachment from the surface. For our purposes, we can also use this as a demarcation point between dense plume and rarified plume. Ion production in a detached (rarified) plume is significantly different from ion production in a quasi-stationary plume that is supported by a continuous evaporation from the solid sample (dense plume). Depending on the mechanism of ion production, this transition may lead to a dramatic change in the ion yield. Model calculations showed that the dense plume phase extended beyond the duration of the laser pulse.[17] We expect to see the effect of the dense to rarified plume transition on the time-resolved ion yield signal.

The objective of the current study was to obtain more reliable data on the ns time scale kinetics of guest ionization. This was achieved by the accurate control of the delay time between the pump and probe pulses and by significantly reducing the signal fluctuations by improving sample homogeneity. Specifically, we were interested in ion yield variations up to 20 ns following the laser pulse. Here, we report the kinetics of MALDI ion formation for protonated substance P and insulin from several commonly used MALDI matrixes.

Experimental Section

TOF Mass Spectrometer. The schematic layout of the instrument used for the MALDI pump−probe studies is shown in Figure 1. Ions were formed by pulsed laser irradiation of a guest-doped matrix layer deposited on a stainless steel probe. The ions were accelerated to 28.0 keV kinetic energy by the ion extraction system and mass separated in a 2.1m-long linear time-of-flight (TOF) mass spectrometer (Comstock Inc., Oak Ridge, TN). A microchannel plate transducer (dual assembly, 25 mm diameter MCP, Galileo, Sturbridge, MA) was used to detect ions. The time-of-flight spectra were recorded by a 1 GHz digital oscilloscope (Model 9370M, LeCroy Corporation, Chestnut Ridge, NY) triggered by a fast photodiode. Data were transferred to a PC and averaged with the help of a custom-made data acquisition package (TOFWARE, Ilys Software, Pittsburgh, PA). The resolution of the mass spectrometer was measured to be ∼400 (fwhm) and was high enough to distinguish sodiated and protonated guest ions. A CCD camera attached to a long-distance microscope (LDM) was used to monitor the position of the laser spots on the sample and to aid in the alignment procedure.

Pump−Probe Arrangement. Laser radiation from a nitrogen laser (VSL-337ND, Laser Science, Newton MA) with 3.5 ns pulse width was split into two beams, direct and delayed, with a 50% beam splitter. A step filter was used to attenuate the direct beam. The proper attenuation was determined experimentally for each matrix-guest mixture to obtain irradiances at the sample below the threshold value for ion generation. To provide stable propagation directions of the direct and delayed beams for different positions of the retroreflector, two iris apertures were used. The position of the 2.2 mm diameter first aperture (AP1) was chosen to provide relatively flat laser intensity distribution in the focal plane. To determine the radial intensity distribution, the diameter of the aperture was varied from 0.6 to 2.2 mm in steps of 0.2 mm, and the transmitted pulse energy was measured by a pyroelectric joulemeter (J4−05, Molectron Detector, Portland, OR). The energy was found to be directly proportional to the iris area with an accuracy of ∼5%, which was indicative of a flat laser intensity distribution.

The maximum time delay between direct and delayed pulses corresponded to a difference in travel distance of ∼5.2 m. Due to its low divergence (0.3 mrad), the laser beam in the delayed channel carried sufficient energy to bring about the formation of guest ions. The direct and delayed beams were merged near the entrance window of the mass spectrometer by a second 50% beam splitter. The combined beam was focused onto the probe surface with a 25 cm focal length lens. To facilitate measuring the pulse energy in either beam, a flipper mount (New Focus, Santa Clara, CA) with a turning mirror was placed in front of the focusing lens.

The optical delay line provided variable time separation between the direct and delayed laser pulses. A retroreflector (Melles Griot, Irvine, CA) was moved along an optical rail (Thorlabs Inc, Newton, NJ) to provide high accuracy delay times between 0.25 ns and 17.2 ns. At different positions of the retroreflector, the laser intensity distribution on the AP2 aperture (1.8 mm diameter) was defined by the beam walkout and by the divergence of the laser beam. The walkout was attributed to parallel displacement of the laser beam due to the inevitable warp of the optical rail. To compensate this effect, the center of the laser spot was aligned with the center of the aperture by fine adjustment of the M2 mirror (see Figure 1). Because of finite laser beam divergence, the laser energy after the second aperture was a function of the retroreflector position. To compensate for this effect, a variable attenuator (935−3-ORT, Newport, Fountain Valley, CA) was incorporated into the delay line. By adjusting the attenuator at different positions of the retroreflector, the laser pulse that passed through the AP2 aperture was kept at constant energy (±2.5%). The distances of apertures AP1 and AP2 from the BS2 beam splitter were chosen equal. By selecting a slightly smaller diameter for the delayed beam, it was possible to minimize the effect of unavoidable beam walking on the overlap of the two beams.

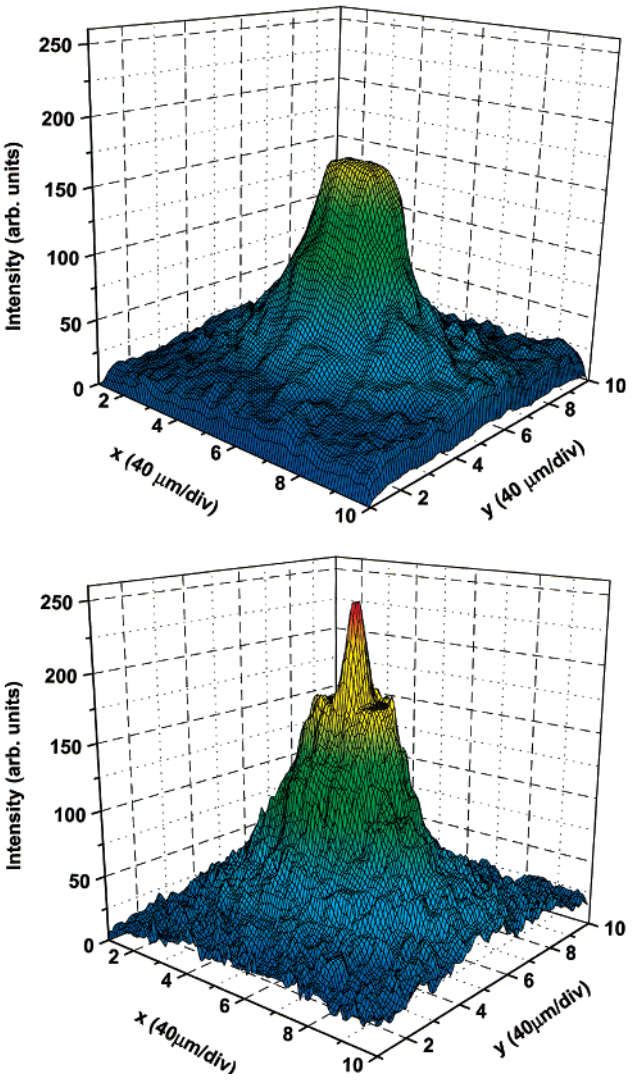

Figure 2. Laser intensity distributions across a/a single pulse and b/the two well aligned overlapping pulses near the surface of the sample. One of the pulses is apertured to fit inside the focal spot of the other pulse to minimize the potential effect of beam walking.

The quality of the beam alignment was examined by inspecting the merged beam cross section right after the BS2 beam splitter and at ~2 m. For a final alignment check, the images of the laser spots on the probe surface were taken by a CCD camera for the delayed, direct, and merged laser beams (see, Figure 2). The elliptical laser spot on the sample had major and minor axes of ~300 μm and ~200 μm, respectively. Typical integral fluences used for MALDI of the different matrixes were in the range of 200−800 J/m^2.

Sample Preparation. Three of the matrixes, 2,5-dihydroxybenzoic acid (DHB), α-cyano-4-hydroxycinnamic acid (CHCA), and 9-anthracenecarboxylic acid (9-ACA), as well as the bovine insulin and substance P guest species were obtained from Sigma (St. Louis, MO). Sinapinic acid (SA) was obtained from Aldrich Chemical Co (Milwaukee, WI). The saturated matrix solutions were prepared fresh daily in 7:3 (v/v) mixture of acetonitrile (HPLC grade from Fisher Scientific, Fair Lawn, NJ) and deionized water (18.2 MΩ×cm). The 1×10^{-4} M bovine insulin and 2×10^{-4} M substance P solutions were prepared in 0.1% trifluoroacetic acid (TFA) (reagent grade from Aldrich, Milwaukee, WI).

Significant improvement in MALDI signal quality and reproducibility was observed when the dried droplet sample preparation method was replaced by electrospray (ES) deposition. To obtain a matrix solution suitable for ES deposition, 100 μL of the saturated matrix solution was mixed with 300 μL of methanol. To prepare the mixture for electrospray deposition, 100 μL of the peptide solution was mixed with 400 μL of the matrix solution. Finally, an electrically isolated syringe was filled with this mixture to deliver a constant flow at a rate of 20 μL/min using a syringe pump. To generate a high throughput electrospray, a stabilized 6.0 kV DC voltage (230−10R, Bertran, Hicksville, NY) was applied to the syringe needle (Type 90584, i.d. = 0.150 mm, Hamilton Company, Reno, NV). Approximately 5 μL of the sample solution was ES deposited on the flat part of the grounded stainless steel probe (5 mm diameter).

Data Collection. Data were collected by averaging single-shot spectra for chosen delay and pulse energy settings. The summed spectrum was obtained adding 200−300 individual spectra at a repetition rate of 1 Hz. The ion yield was obtained by integrating the area of the singly charged peptide peak. No ions with higher charge were observed in this study. The probe was continuously rotated to provide fresh sample surface for every laser shot.

The dependence of the ion yield on laser energy was obtained for each guest/matrix mixture before determining the spectra at different delays. This helped us to find the energy setting necessary to keep the individual pulses below the threshold for MALDI ion generation. By definition, at threshold energy MALDI signal was produced in ~50% of the laser shots with an amplitude at least three times over the background noise.

Results and Discussion

The difficulties of determining MALDI ion yields are mainly related to the very high degree of sample inhomogeneity. Upon scanning a dried droplet sample surface with the laser, the ion yields can vary by a factor of 2 to three. Because ES deposition significantly diminished these variations,[18] it becomes possible to unambiguously observe the changes in the yield of the MALDI ions caused by changes in laser parameters. Despite the fact that even with ES deposited samples shot-to-shot variations could reach 30 to 50%, averaging ~100 mass spectra taken from spots across the sample gave consistent results.

The direct and delayed pulse irradiances had to be below the ion generation threshold. To accurately set these irradiance values, the guest ion yield, Y_g, had to be measured as a function of the laser pulse energy, E. Figure 3 demonstrates the dependence of the ion yield of protonated guest ions (insulin or substance P) on laser energy. The experiments were performed for four different guest/matrix mixtures: insulin in SA and substance P in CHCA, DHB and 9-ACA. The ion yield was obtained by determining the peak area in a window positioned around the time-of-flight of the guest ions. The laser energy dependence of the ion yield showed the familiar power law, $Y_g \propto E^p$,[19] with the exponents in the $5.0 < p < 7.4$ range (see the caption of Figure 3). An upper limit for the threshold laser energy for MALDI ion generation, E_{thr}, was measured for all four matrix/guest mixtures. Since in the pump−probe experiments only $\sim 0.7 \times E_{thr}$ pulse energy was used, it was sufficient to determine the upper limit for the threshold.

It is interesting to notice that the CHCA based system shows significantly lower threshold and substantially higher ion yields than the systems based on the other matrixes. This behavior is in agreement with our earlier observations for the relative guest ion yield of glycine homologues, Gly_n in various matrixes.[9] In that study, the ion yields, significantly higher in CHCA than in

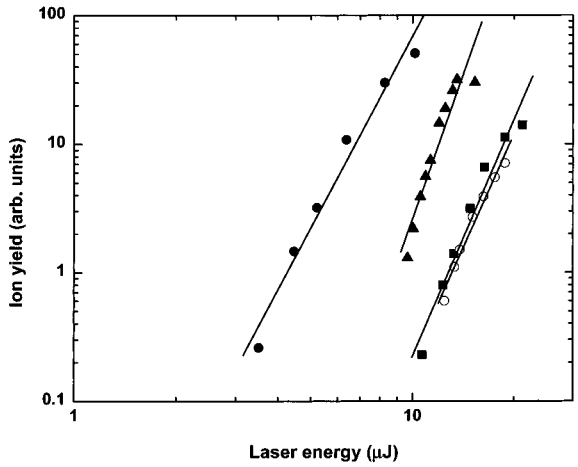

Figure 3. Guest molecular ion yield in different matrixes as a function of laser energy (● substance P in CHCA, $p = 5.0 \pm 0.4$; ▲ insulin in SA, $p = 7.4 \pm 0.9$; ■ substance P in DHB $p = 6.1 \pm 0.6$ and ○ substance P in 9-ACA $p = 5.8 \pm 0.4$).

SA, were attributed to the markedly lower proton affinity (PA) of the CHCA (183 ± 2 kcal/mol) compared to that of SA (204 ± 4 kcal/mol).[20] One could argue that proton transfer from the ground state of the protonated CHCA to the guest molecule occurred more readily than from the protonated SA due to the ~21 kcal/mol advantage in the PA balance.

Figure 4a demonstrates the delay time dependence of the guest ion yield for two mixtures: insulin in sinapinic acid (SA) and substance P in DHB. The curves for these mixtures were found to follow exponential decay with characteristic times 4.3 ± 0.7 ns for substance P in DHB and 4.6 ± 0.8 ns for insulin in SA. The decay curves for the rest of the guest/matrix mixtures are shown in Figure 4b. It is clear that the major feature of curves in Figure 4b is the extended domain of ion production at intermediate delays. The width of this domain was found to be approximately 5 ns for substance P in 9-ACA and at least 14 ns for substance P in CHCA. The simplest model for this type of kinetic behavior is based on two consecutive reactions (see the analysis later). In all cases, the drop in guest signal was accompanied by a reduction of matrix ion yield.

There are two nonkinetic factors to consider for the explanation of the ion yield curves in Figure 4a. First, the time resolution of the experiment is limited by the length of the laser pulse (3.5 ns). Thus, processes with characteristic times below 3.5 ns are not accessible with the nitrogen laser. Even the two exponential decay curves in Figure 4a ($\tau = 4.3 \pm 0.7$ ns for substance P in DHB and $\tau = 4.6 \pm 0.8$ ns for insulin in SA) are considered borderline cases. The decay can be explained by the relaxation of the excited matrix molecules, as well as by the diminishing overlap between the two laser pulses. In the case of DHB, fluorescence data suggests ~5 ns relaxation time for the excited state[14] but our ion yield data obtained at 30 ps time resolution[16] indicates a faster and more complex decay.

The second effect is present because the ionization processes in a MALDI plume occur in an expanding environment. Hydrodynamic calculations show that during the first 10 ns the plume expands to a distance of ~8 μm from the surface and due to the continuous supply of material from the solid the plume density remains close to the condensed phase value (dense plume).[17] By 100 ns, the plume detaches from the surface, it expands to ~60 μm and its density drops to ~1/10-th of the solid-phase value (rarified plume). Thus, ion yield changes during the first ~10 ns stem mostly from the kinetics of ionization and only to a lesser degree from the volume changes

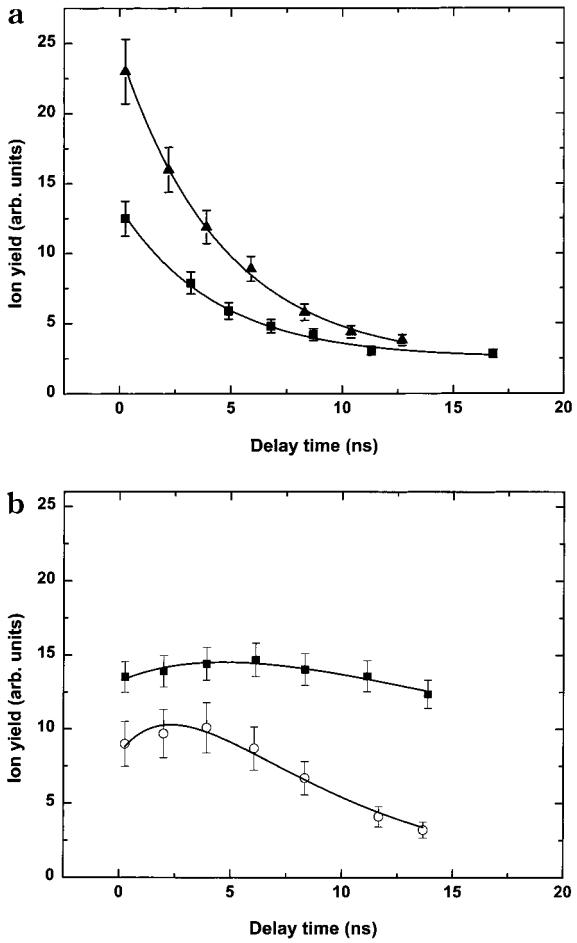

Figure 4. (a)Yield of guest ions for insulin in sinapinic acid (▲) and substance P in DHB (■) as a function of delay time between the pump and the probe laser pulses. A simple exponential decay can be modeled as first-order kinetics in both cases. The decay times are $\tau = 4.3 \pm 0.7$ ns for substance P in DHB and $\tau = 4.6 \pm 0.8$ ns for insulin in SA. (b)Yield of guest ions for substance P in CHCA (●) and in 9-ACA (○) matrixes as a function of the delay time. The fitted curves are based on ion formation from the intermediate product in two consecutive first-order reactions with $\tau_1 = 31$ ns and $\tau_2 = 5.6$ ns for CHCA and $\tau_1 = 7.0$ ns and $\tau_2 = 3.0$ ns for 9-ACA (see text).

resulting in precursor concentration changes. Given the time resolution of our system, we expect to be able to distinguish between processes occurring in the dense plume ($T_{surf} > T_{subl}$) and rarified plume ($T_{surf} < T_{subl}$). How fast after the end of the laser pulse this transition occurs depends on the dynamics of heat dissipation. Both heat conduction toward the bulk of the sample and evaporative cooling at the surface help the temperature to drop. The key material parameters determining how fast the transition takes place are the thermal conductivity of the sample and the heat of vaporization of the matrix. In case of SA and DHB (Figure 4a), the dense plume ceases to exist at the end of the laser pulse or its presence is not the rate-limiting factor in producing the guest ions. This scenario could be consistent with the ESPT mechanism.

Due to the expanding plume environment, studying the delay time dependence of the ion yield for matrix and guest ions gives insight into the relative importance of processes occurring in the condensed phase, in the dense and in the rarified plume (see Figure 5). Subnanosecond changes in the ion yield correlate with condensed phase phenomena (e.g., exciton pooling, phase transition). According to molecular dynamics calculations, a phase transition occurs at ~60 ps after the start of the laser heating.[21] Ion yield variations between ~1 ns and ~10 ns can

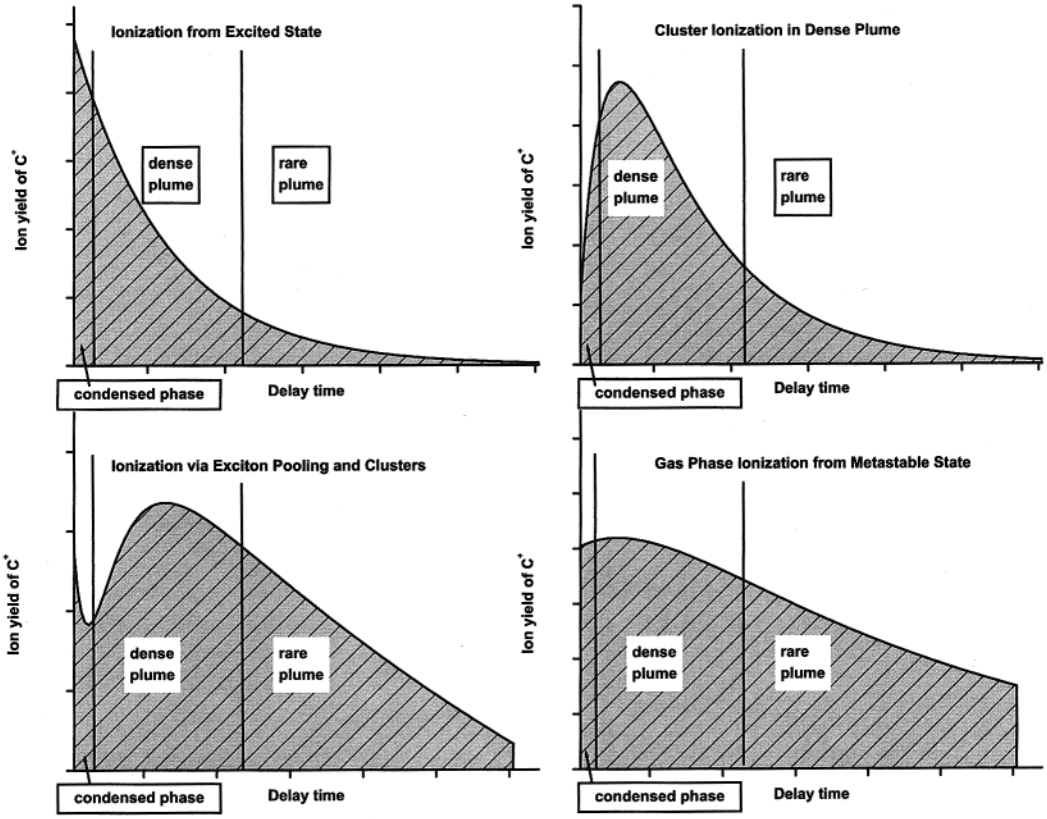

Figure 5. Ion yield kinetics are shown for different ion formation mechanisms in an expanding plume. Ionization from an excited state (top left), cluster ionization in the dense plume (top right), gas-phase ionization from a metastable state (bottom right) and ionization via exciton pooling and clusters (bottom left) can be distinguished.

be linked to processes in the dense plume, whereas changes on longer time scales (>10 ns) are primarily due to events in the expanded plume.

Measuring the delay time dependence of the ion yield provides information on the production mechanism. Figure 5 shows four examples of ion yield kinetics and their possible interpretation. The top left panel shows direct ionization from an excited state with a single relaxation time for the excited state. The top right panel describes the ion production in the case when ions are formed in the dense plume possibly mediated by clusters. Clearly, in this case, the maximum ion yield is observed during the existence of the dense plume. A more complex mechanism is apparent in the bottom left panel. In this case, both condensed phase processes (e.g., exciton pooling) and plume reactions are important. The bottom right panel depicts a situation when a metastabile state and gas-phase ionization are not negligible.

To find a simple fit for the ion yield data in Figure 4b, an exponential decay curve was selected consistent with the assumption of two consecutive reactions

$$Y_g = A_1 e^{-t/\tau_1} - A_2 e^{-t/\tau_2}$$

where t is the delay time, A_1 and A_2 are the amplitudes and τ_1 and τ_2 are the characteristic times of the reactions. As it is seen in Figure 4b, good fit can be found for both sets of ion yield data. For substance P in 9-ACA $\tau_1 = 7.0$ ns and $\tau_2 = 3.0$ ns, whereas for substance P in CHCA $\tau_1 = 31$ ns and $\tau_2 = 5.6$ ns.

Inspecting Figure 4, it is quite clear that the kinetics of guest ion formation in CHCA is significantly different from other matrixes such as 9-ACA and especially SA and DHB. Similar anomalies were observed for CHCA in the guest ion yield as a function of laser pulse energy (see Figure 3) and in the relative ion yield of Gly_n ($n = 1$ to 6).[9] In searching for an explanation, one needs to consider the length of the dense plume regime and the competition for the proton between the guest and the matrix species.

Let us assume that the guest ions are formed relatively fast, i.e., simultaneously with the laser excitation, and lift off the surface with the expanding plume. Because the desorption threshold for the matrix is much lower, the desorbed guest ions move through the dense gas of neutrals, experience multiple collisions, and, thus, gain temperature. The longer the dense plume regime lasts, the more stretched is the plume. Thus, during their travel with the dense plume, the guest ions can lose the proton to other species. The rate of deprotonation is a function of temperature, density and proton affinities of both the guest and the matrix. The dynamics of deprotonation may be complex. As a first approximation, we can assume that the temperature of the top layers for each matrix is similar, and so is the plume density. The removal of proton donors (protonated guest ions) from the plume is then governed by proton affinities of the proton acceptor species. Because the rate of proton loss is proportional to the number of collisions with proton acceptors per unit length traveled by the guest ions, the ion yield will decay exponentially with the traveled distance. Therefore, with the longer dense plume regimes resulting in more stretched plumes, the probability of guest ion survival follows an exponential decay, with the exponent dependent on the PA of matrix.

In this scenario, CHCA, the matrix with the lowest PA, presents possibilities for the guest ions to lose their proton to the neutral matrix molecules. This may be the reason the protonated substance P is observable at longer delays in CHCA matrix. Eventually, when the delay is too long, the excitation of the top sample layer drops by the time of the second pulse

arrival, thus, the guest ion production is reduced. The observation of strong guest ion signal at maximum delay time from CHCA matrix indicates that the excitation of the surface of the sample is still sufficient to support a steady stream of precursors.

Our pump−probe MALDI experiments have enabled us to separate two dramatically different regimes of ion formation. In the first case (SA and DHB), the guest ionization is determined by the availability of excited matrix species. Due to the fast relaxation of the excited matrix molecules ($t = 5$ns for DHB) guest ionization follows a similarly fast relaxation. In the case of 9-ACA and especially CHCA, the guest ions are continuously released from the sample as long as the surface temperature is above the matrix sublimation temperature. Competition for the proton in the plume between the guest and matrix species can be important as it is indicated by the low PA of CHCA and the high guest ion yields from this matrix. To clarify the rate-limiting step in the rate of guest ion formation from SA and DHB matrixes better time resolution is needed. We plan to continue these experiments using a frequency tripled mode locked Nd:YAG laser.

In our discussions with T. J. Cornish, it was pointed out that the above results have significant bearing on the design of miniaturized MALDI TOF mass spectrometers.[22] As the size of the ion source is reduced in these systems, the residence time in the accelerating region becomes comparable to the ion formation times for CHCA and 9-ACA. This leads to limitations in mass resolution for miniaturized TOF mass spectrometers. On the basis of our data, it is expected that this limitation is significantly less pronounced for DHB and SA. Further studies of fast ionization dynamics promise to provide additional help with the development of miniaturized ion sources.

Acknowledgment. The authors express their gratitude to R. Knochenmuss and to R. Zenobi of the Swiss Federal Institute of Technology Zurich (ETH Zentrum), Zurich, Switzerland, for fruitful discussions on mechanistic issues. We are also thankful to T.J. Cornish of the Johns Hopkins University Applied Physics Laboratory, Laurel, MD, for pointing out the relevance of these studies to the design of miniaturized MALDI TOF mass spectrometers. Financial support for this research from the National Science Foundation (CHE-9873610) and from the Department of Energy (DE-FG02-01ER15129) is gratefully acknowledged.

References and Notes

(1) Zenobi, R.; Knochenmuss, R. *Mass Spectrom. Rev.* **1998**, *17*, 337.
(2) Karbach, V.; Knochenmuss, R. *Rapid Comm. Mass Spectrom.* **1998**, *12*, 968.
(3) Heise, T.; Yeung, E. *Anal. Chim. Acta* **1995**, *299*, 377.
(4) Chen, X.; Carrol, J.; Beavis, R. *J. Am. Soc. Mass Spectrom.* **1998**, *9*, 885.
(5) Gimon, M. E.; Preson, L. M.; Solouki, T.; White, M. A.; Russell, D. H. *Org. Mass Spectrom.* **1992**, *27*, 827.
(6) Chiarelly, M. P.; Sharkey, A. G.; Hercules, D. M. *Anal. Chem.* **1993**, *65*, 307.
(7) Preston-Schaffer, L. M.; Kinsel, G. R.; Russell, D. H. *J. Am. Soc Mass Spectrom*. **1994**, *5*, 800.
(8) Juhasz, P.; Costello, C. *Rapid Comm. Mass Spectrom*. **1993**, *7*, 343.
(9) Olumee, Z.; Vertes, A. *J. Phys. Chem. B* **1998**, *102*, 6118.
(10) Ehring, H.; Karas, M.; Hillenkamp, F. *Org. Mass Spectrom*. **1992**, *27*, 472.
(11) Wang, B. H.; Dreisewerd, K.; Bahr, U.; Karas, M.; Hillenkamp, F. *J. Am. Soc. Mass Spectrom*. **1993**, *4*, 393.
(12) Land, C. M.; Kinsel, G. R. *Eur. Mass Spectrom.* **1999**, *5*, 117.
(13) Land, C. M.; Kinsel, G. R. *J. Am. Soc. Mass Spectrom.* **1998**, *9*, 1060.
(14) Ehring, H.; Sundqvist, B. U. R. *J. Mass Spectrom.* **1995**, *30*, 1303.
(15) Tang, X.; Sadeghi, M.; Olumee, Z.; Vertes, A. *Rapid Comm. Mass Spectrom*. **1997**, *11*, 484.
(16) Knochenmuss, R.; Vertes, A. *J. Phys. Chem. B* **2000**, *104*, 5406.
(17) Vertes, A.; Irinyi, G.; Gijbels, R. *Anal. Chem.* **1993**, *65*, 2389.
(18) Hensel, R. R.; King, R. C.; Owens, K. G. *Rapid Comm. Mass Spectrom.* **1997**, *11*, 1785.
(19) Ens, W.; Mao, Y.; Mayer, F.; Standing, K. G. *Rapid Comm. Mass Spectrom.* **1991**, *5*, 117.
(20) Burton, R. D.; Watson, C. H.; Eyler, J. R.; Lang, G. L.; Powell, D. H.; Avery, M. Y. *Rapid Commun. Mass Spectrom.* **1997**, *11*, 443.
(21) Sadeghi, M.; Wu, X.; Vertes, A. *J. Phys. Chem. B* **2001**, *105*, 2578.
(22) Cornish, T. J., private communication, 2001.